Photophysical property and optical nonlinearity of cyclo[18]carbon (C_{18}) precursors, C_{18}-$(CO)_n$ (n = 2, 4, and 6): Focusing on the effect of carbonyl (-CO) groups

Xia Wang [a], Zeyu Liu [a,*], Xiufen Yan [a], Tian Lu [b,*], Haowei Wang [a], Weiwei Xiong [a,*]

[a]*School of Environmental and Chemical Engineering, Jiangsu University of Science and Technology, Zhenjiang 212100, People's Republic of China*

[b]*Beijing Kein Research Center for Natural Sciences, Beijing 100022, People's Republic of China*

[*]Corresponding author. E-mail: liuzy@just.edu.cn (Zeyu Liu); sobereva@sina.com (Tian Lu); xiongweiwei@just.edu.cn (Weiwei Xiong)

Abstract

Considering their remarkable chemical stability, the precursors of cyclo[18]carbon (C_{18}), C_{18}-$(CO)_n$ (n = 2, 4, and 6), have more practical significance than the elusive C_{18} ring. In the present paper, the electronic spectrum and (hyper)polarizability of the C_{18}-$(CO)_n$ (n = 2, 4, and 6) are studied by theoretical calculations and analyses for revealing the utility of introduction of carbonyl (-CO) groups on molecular optical properties. The analysis results show that the successive introduction of -CO groups leads to red-shift of the absorption spectrum, but maximum absorption of all molecules is mainly due to the charge redistribution caused by electron transition within C_{18} ring. Except for the vanishing first hyperpolarizability of C_{18}-$(CO)_6$ results from its octupolar character, the (hyper)polarizabilities of the precursors present an ascending trend with the increase of -CO groups in the molecule, and the higher-order response properties are more sensitive to the number of -CO groups. By means of (hyper)polarizability density analysis and (hyper)polarizability contribution decomposition, the fundamental reasons for the difference of (hyper)polarizability of different molecules were systematically discussed from the perspectives of physical and structural origins, respectively. As to the frequency dispersions under the incident light, the significant optical resonances were found on the hyperpolarizability of molecules C_{18}-$(CO)_n$ (n = 2, 4, and 6), which contrast with the fact that it has inconspicuous influences on molecular polarizability.

Table of contents (TOC) graphic:

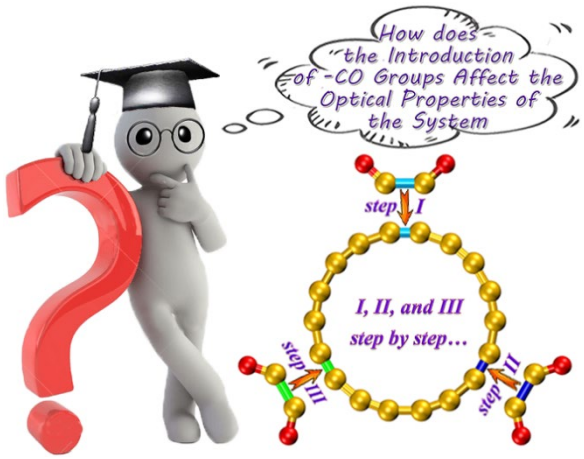

1. Introduction

Since Hoffmann first proposed the idea of cyclocarbons in 1966 [1], people have been exploring how to obtain an all-carboatomic ring with sp-hybridization [2-6]. After successfully induced skeleton rearrangement through atom manipulation to generate linear carbon chains with terminated benzene rings in 2018 [7], Kaiser and co-workers realized, for the first time, the gen and characterization of the cyclocarbon consisting of 18 doubly coordinated carbon atoms, known as cyclo[18]carbon (C_{18}), using the similar technology [8]. Due to its novel geometric configuration and special electronic structure, large numbers of theoretical studies on this allotropic carbon have been reported successively since it was prepared experimentally [9-23]. However, the high activity makes C_{18} molecule has not been stably isolated so far [2,8,24], which becomes an unavoidable obstacle for its practical application in functional materials.

The organic precursor of the seminal experiment for the generation of C_{18} is the cyclocarbon oxide molecule C_{18}-$(CO)_6$, and the preparation process is to remove the masking carbonyl groups (-CO) from it sequentially [8]. Two other novel carbon-rich molecules with cyclic skeleton, C_{18}-$(CO)_4$ and C_{18}-$(CO)_2$, are usually emerged as chemical intermediates, and the final all-carboatomic C_{18} ring can be formed in one or more steps. It was found from some experimental explorations that C_{18}-$(CO)_6$ is an easily synthesized and relatively stable species under ambient conditions [25,26], and researchers even determined its crystal structure by X-ray diffraction very early [26].

Modifying the molecular skeleton with different numbers and/or varieties of substituents has been proved to be a very effective way to change the electronic structure of a system [27]. For a series of cyclocarbon oxides C_{18}-$(CO)_n$ (n = 2, 4, and 6), it is just equivalent to introducing several electron-accepting -CO groups with strong electron-withdrawing ability into the carbon ring, so their multiple properties are expected to be fundamentally distinct from those of the C_{18}. Although the theoretical studies on various physicochemical properties and behaviors of C_{18} ring and its analogues have been quite extensive [9-23], the research on the precursors C_{18}-$(CO)_n$ (n = 2, 4, and 6) for manufacturing C_{18} has not been fully carried out. As

far as we know, only our latest work has systematically studied and comparatively analyzed bonding character, electron delocalization, and aromaticity of relevant systems up to now [28]. The results show that C_{18}-$(CO)_n$ (n = 2, 4, and 6) possess two perpendicular π-conjugated electron systems, in-plane and out-of-plane π molecular orbitals (MOs), similar to the C_{18} ring. Importantly, the number of -CO groups is closely related to π conjugation in the molecule, and therefore affects their overall aromaticity. Our another theoretical research has revealed that C_{18} ring shows strong absorption spectrum and significant optical nonlinearity, indicating its potential as an advanced optical material [11]. Given these facts, a question naturally arises as to how do the sequential grafting of -CO groups change the optical properties of C_{18}? This is the very focus of the current paper.

In this work, the electronic absorption spectrum and nonlinear optical (NLO) properties of the cyclocarbon oxide precursors of C_{18}, C_{18}-$(CO)_n$ (n = 2, 4, and 6), are explored in depth by employing density functional theory (DFT) calculations and wavefunction analysis methods. The influence and regulation of the number of -CO groups on the optical properties of the molecule are focused on, and the essential reason for the significant difference in related properties is unveiled.

2. Computational Details

The geometric structures and excitation characteristics of the C_{18}-$(CO)_n$ (n = 2, 4, and 6) were respectively obtained by DFT and time-dependent DFT (TD-DFT) calculations at ωB97XD [29]/def2-TZVP [30] level in the gas phase. Our recent theoretical work has demonstrated that this computational strategy can reproduce the crystal structure of C_{18}-$(CO)_6$ well, so it is considered to be competent to describe the present systems [28]. The molecular (hyper)polarizabilities were calculated by both analytic derivatives of the system energy [namely, coupled-perturbed Kohn-Sham (CPKS)] and finite field (FF) methods at the ωB97XD/aug-cc-pVTZ(-f,-d) level, where aug-cc-pVTZ(-f,-d) is a reduced version of the aug-cc-pVTZ basis set [31] with the removal of *f*-type polarization functions of non-hydrogen atoms and *d*-type

polarization functions of hydrogen atoms. The (hyper)polarizability densities were evaluated at the same level. For detailed formulas for calculating molecular response properties, please refer to Ref. [10,11].

Gaussian 16 (A.03) program package was utilized for all quantum chemistry calculations [32]. Multiwfn 3.8(dev) code was employed to perform the electronic structure analyses and plot charge-transfer spectrum (CTS) based on the output and formatted check point files of Gaussian 16 [33,34]. The unit sphere representation and local contribution map of (hyper)polarizabilities were rendered by means of Visual Molecular Dynamics (VMD) software [35] based on the files exported from Multiwfn 3.8(dev). The colored contour maps of local contribution of (hyper)polarizabilities were plotted directly via Multiwfn 3.8(dev).

3. Results and Discussion

The geometric structures of the precursors C_{18}-$(CO)_n$ (n = 2, 4, and 6) without imaginary frequency are shown in **Fig. 1**. For corresponding Cartesian coordinates, please refer to the supplementary material of Ref. [28]. All precursors are observed to be strictly planar, and molecules with n = 2, 4, and 6 belong to C_{2v}, C_{2v}, and D_{3h} point groups, respectively.

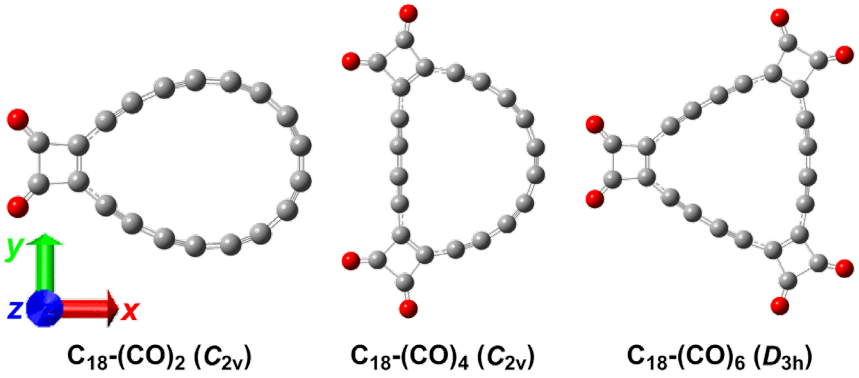

Fig. 1. Geometric structure of C_{18}-$(CO)_n$ (n = 2, 4, and 6) studied in the present work. C atoms are in gray and O atoms are in red. Also shown is the Cartesian axis used for defining the component of molecular response properties.

3.1 Photophysical Property: Electronic Absorption Spectrum

The absorption spectrum can reflect the structure and motion of molecules in the system, as well as their electronic transition behavior under the action of electromagnetic field [36-38]. As readily observed from **Fig. 2**, there exists significant difference in the absorption band of the three precursors C_{18}-$(CO)_n$ (n = 2, 4, and 6). The C_{18}-$(CO)_2$ shows only one absorption peak of 225.0 nm in ultraviolet-visible (UV-Vis) region. In contrast, the absorption peak of C_{18}-$(CO)_4$ blue-shifted to 215.9 nm, and there appears a new weak absorption at 294.5 nm. For molecule C_{18}-$(CO)_6$, compared with the other two precursors, its strong absorption continues to move toward short wavelength to 209.0 nm, accompanied by the enhancement of the weak absorption and red-shift to 344.0 nm.

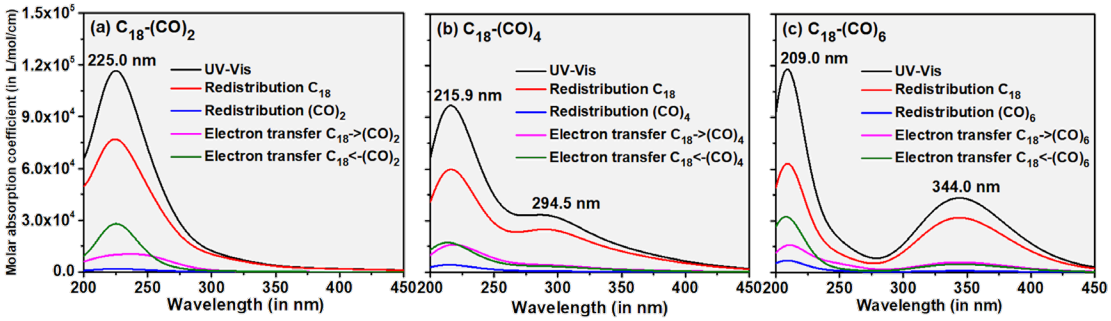

Fig. 2. Simulated absorption spectrum and CTS of C_{18}-$(CO)_n$ (n = 2, 4, and 6). A Gaussian function with a full width at half-maximum (FWHM) of 3500 cm^{-1} was employed for broadening the theoretically calculated data as spectrum curve.

In order to understand the essence of electron excitation from the perspective of charge transfer, CTS is employed to graphically present the contribution of charge redistribution within fragment (intrafragment local excitation) and charge transfer between fragments to the absorption spectrum of the C_{18}-$(CO)_n$ systems [34,39]. We divided the C_{18}-$(CO)_n$ (n = 2, 4, and 6) into two fragments, the C_{18} moiety and the -$(CO)_n$ (n = 2, 4, and 6) group, and the corresponding CTSs were drawn into the colored curves in **Fig. 2**. As one can see, the electron redistribution inside the C_{18} ring comprises a decisive proportion of optically active electron excitations, while the electron redistribution inside the -$(CO)_n$ (n = 2, 4, and 6) group is almost negligible. The contributions of electron transitions within and between the fragments of three molecules to the overall absorption spectrum generally show the following trend:

electron redistribution inside the C_{18} ring > electron transfer from the -$(CO)_n$ group to the C_{18} ring > electron transfer from the C_{18} ring to the -$(CO)_n$ group > electron redistribution inside the -$(CO)_n$ group. The prominent interfragment transition character implies strong coupling between the C_{18} ring and the -$(CO)_n$ group.

3.2 Optical Nonlinearity: Static and Dynamic (Hyper)Polarizabilities

Molecular (hyper)polarizabilities are response properties of a molecule to an external electric field, which determine the NLO performance of molecular materials. The polarizability reflects the change in molecular dipole moment caused by applying unit electric field, while the molecular hyperpolarizability represents its nonlinear polarization effect. The calculated (hyper)polarizabilities of C_{18}-$(CO)_n$ (n = 2, 4, and 6) including the isotropic average polarizability [$\alpha_{iso}(\lambda)$], the projection of first hyperpolarizability on molecular dipole [$\beta_{vec}(\lambda)$], and the average of second hyperpolarizability [$\gamma_{||}(\lambda)$] in zero-frequency limit (λ = ∞ nm) and under frequency-dependent fields (λ = 1907, 1460, 1340, 1180, and 1064 nm), which can be compared with experimental observations or deductions, will be comprehensively discussed in the following sections. Their axial tensorial components are given in **Tables S1** and **S2**.

3.2.1 Static (Hyper)Polarizabilities

It can be seen from **Fig. 3** that except for the first hyperpolarizability [$\beta_{vec}(\infty)$] of the C_{18}-$(CO)_6$ molecule, the values of static (hyper)polarizabilities present an ascending trend with the increase of the number of -CO groups in the molecule. The C_{18}-$(CO)_6$ exhibits the first hyperpolarizability [$\beta_{vec}(\infty)$] of zero because it is a standard octupolar molecule with D_{3h} symmetry. The higher-order response properties of molecules are more susceptible by the number of -CO groups than the lower-order ones. Specifically, the second hyperpolarizability [$\gamma_{||}(\infty)$] of the precursors increases significantly with the number of -CO groups, while the change in molecular polarizability [$\alpha_{iso}(\infty)$] is relatively less obvious.

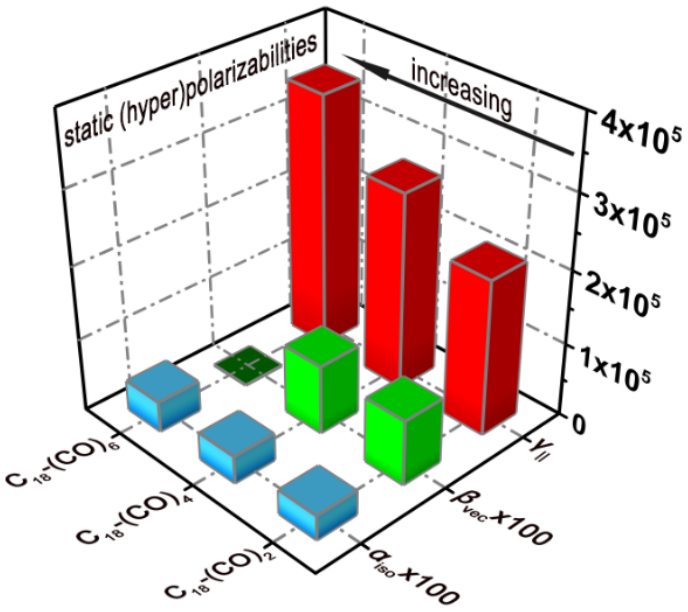

Fig. 3. Isotropic average polarizability [$\alpha_{iso}(\infty)$], projection of first hyperpolarizability on molecular dipole [$\beta_{vec}(\infty)$], and average of second hyperpolarizability [$\gamma_{||}(\infty)$] of C_{18}-$(CO)_n$ (n = 2, 4, and 6) in zero-frequency limit (λ = ∞ nm). The (hyper)polarizabilities are given in au.

Generally, the polarizability of homologous molecules is positively correlated with the molecular volume [40], so the electronic spatial extent ($<R^2>$) which usually used to represent the electron density volume of a molecule can provide a reasonable explanation for the magnitude of the molecular polarizability. The electronic spatial extent ($<R^2>$) and polarizabilities [$\alpha_{iso}(\infty)$] of the C_{18}-$(CO)_n$ (n = 2, 4, and 6) are collectively plotted in **Fig. S1**, from which it can be seen that the polarizabilities of the molecules are almost linearly related to their volumes. Similar conclusion has been found in our recent study on the relationship between the polarizability and molecular volume of various all-carboatomic rings [10].

It should be noted that the calculated polarizability [$\alpha_{iso}(\infty)$] of the C_{18}-$(CO)_n$ for n = 2, 4, and 6 are 1.1, 1.3, and 1.4 times, respectively, that of the free C_{18} ring (293.9 au), and the values are observed to be 1.5, 1.9, and 2.5 times for the second hyperpolarizability [$\gamma_{||}(\infty)$, 140909 au for C_{18}] [9,10], which show that these precursors are better candidates for high-performance optical materials than the C_{18} molecule, and moreover, the number of -CO groups in them plays a crucial role in

determining their (hyper)polarizability.

The unit sphere representation method of (hyper)polarizabilities, which can visually exhibit the characteristics of molecular response properties in terms of (hyper)polarizability tensors, is a powerful means for comprehensive characterization of molecular (hyper)polarizabilities [41]. The unit sphere representation of the (hyper)polarizabilities of C_{18}-$(CO)_n$ (n = 2, 4, and 6) in the static field are depicted in **Fig. 4**. It can be seen that the (hyper)polarizability tensorial components of C_{18}-$(CO)_n$ (n = 2, 4, and 6) are mainly distributed in the molecular plane (XY-plane), while the component perpendicular to the molecular plane (Z-axis) is insignificant, which is reflected by the difference in length and color of vector arrows in each direction. More detailed analysis indicates C_{18}-$(CO)_2$ and C_{18}-$(CO)_4$ exhibit strong polarization and second polarization responses in the directions of their respective molecular long-axis [X-axis of C_{18}-$(CO)_2$ and Y-axis of C_{18}-$(CO)_4$], as shown in **Figs. 4(a)**, **4(b)**, **4(g)**, and **4(h)**, indicating that the molecular long-axis is the most polarizable direction. However, due to the octupolar molecular nature of the C_{18}-$(CO)_6$, its polarizability and second hyperpolarizability in **Figs. 4(c)** and **4(i)** display the same magnitude in all directions on the molecular plane. As can be seen by comparing **Figs. 4(d)**, **4(e),** and **4(f)**, for the molecular first hyperpolarizability, the different geometry of the three molecules leads to obviously diverse but highly regular distribution of hyperpolarizability tensor. The molecules C_{18}-$(CO)_n$ (n = 2, 4, and 6) are found to have n pairs of characteristic induced second-harmonic-generation (SHG) regions under induction of external electric fields. We highlighted all these important areas with thick arrows in **Fig. 4**. When two external electric fields (EEFs) are applied along one of the thick cyan arrows, a significant induced dipole moment will appear in the opposite direction, while an induced dipole in the same direction is expected to occur if two EEFs are exerted simultaneously along one thick purple arrow. The length of the arrow perpendicular to each other in the center of the unit sphere representation exhibit the component of the (hyper)polarizability in Cartesian axis, which clearly show the relative overall magnitudes of (hyper)polarizability along

different axes.

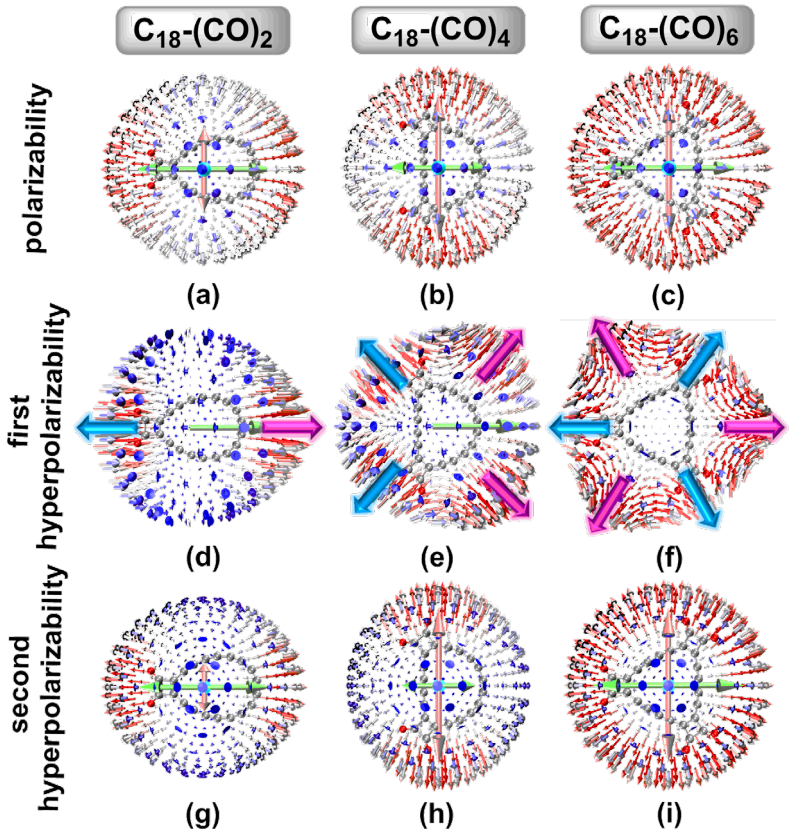

Fig. 4. Unit sphere representation of (hyper)polarizabilities for C_{18}-$(CO)_n$ (n = 2, 4, and 6) in static electric field. Longer and redder radial arrow indicates a larger tensor value in corresponding direction (see main text for the meaning of the thick arrows).

As shown in **Tables S1** and **S2**, with regard to molecular polarizability and second hyperpolarizability, the X-axis tensorial components of C_{18}-$(CO)_2$ and the Y-axis tensorial components of C_{18}-$(CO)_4$ account for the main contribution to the response properties. However, the tensorial components of the polarizability and second hyperpolarizability of molecule C_{18}-$(CO)_6$ are exactly equal for X- and Y-axes. Since their molecular orientation is set to be symmetrical about the X-axis as shown in **Fig. 1**, the three molecules only have a nonvanishing first hyperpolarizability component along the X-axis, while the components in directions of other two axes (Y- and Z-axes) are zero. The (hyper)polarizability tensorial components listed in **Tables S1** and **S2** mutually confirm the correctness of the conclusion drawn from the molecular (hyper)polarizability tensor map in **Fig. 4**. Therefore, we will focus on those tensorial components that contribute most to the overall (hyper)polarizabilities of the molecules

in the following discussion.

The axial tensorial components of the (hyper)polarizability of C_{18}-$(CO)_n$ (n = 2, 4, and 6) obtained by the FF method are listed in **Table S3**. An intuitive comparison of them with the values derived analytically by CPKS method in **Tables S1** and **S2** is drawn in **Fig. 5**. It can be seen that there is almost no distinction in the calculated values of (hyper)polarizabilities between the two methods. Therefore, the reliability of the (hyper)polarizability density analysis and the decomposition of (hyper)polarizabilities to fragment contributions based on the FF method is fully guaranteed.

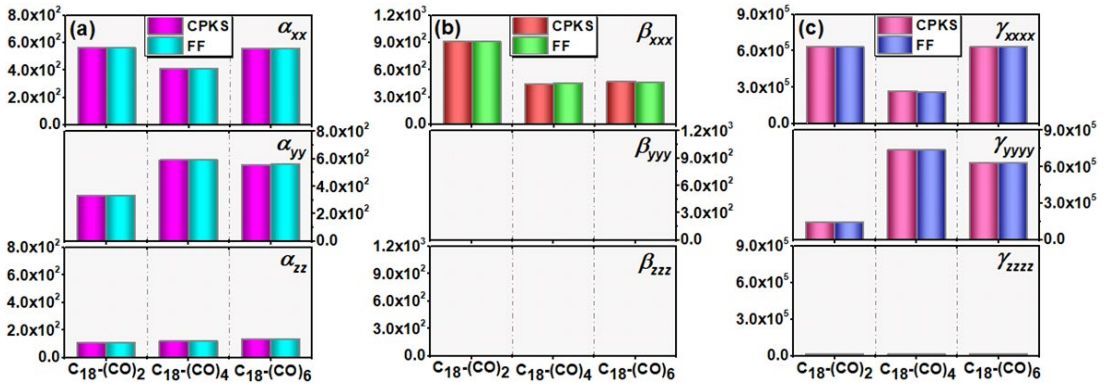

Fig. 5. The tensorial component of (a) polarizability, (b) first hyperpolarizability, and (c) second hyperpolarizability for C_{18}-$(CO)_n$ (n = 2, 4, and 6) calculated by the CPKS and FF (with step size of 0.0001 au) methods, respectively. The (hyper)polarizabilities are given in au.

The (hyper)polarizability density exhibits local contributions of different spatial regions to (hyper)polarizability, which is helpful in understanding the physical essence of molecular response properties [11,36-39,42]. The local contributions to the (hyper)polarizability of the C_{18}-$(CO)_n$ (n = 2, 4, and 6) in direction with their largest tensorial component under zero-frequency field are rendered in **Fig. 6**. These isosurface maps clearly display the regions having positive or negative contribution to molecular (hyper)polarizabilities. For polarizability and second hyperpolarizability densities of C_{18}-$(CO)_n$ (n = 2, 4, and 6), as shown in **Figs. 6(a)-6(c)** and **6(g)-6(i)**, the positive contribution regions (blue isosurfaces) occupy evidently wider spatial range relative to the negative regions (red isosurfaces). This explains why the calculated

major (hyper)polarizability tensorial components given in **Tables S1** and **S2** are very large positive values. In contrast, the isosurfaces of the first hyperpolarizability density of all the three precursors in **Figs. 6(d)-6(f)** are visually scattered, and the positive and negative contribution regions do not show a distinct difference. The color-filled contour maps on molecular plane (XY-plane) of these local contribution maps of (hyper)polarizability in **Fig. S2** provide supplementary information on the intrinsic details of the (hyper)polarizabilities.

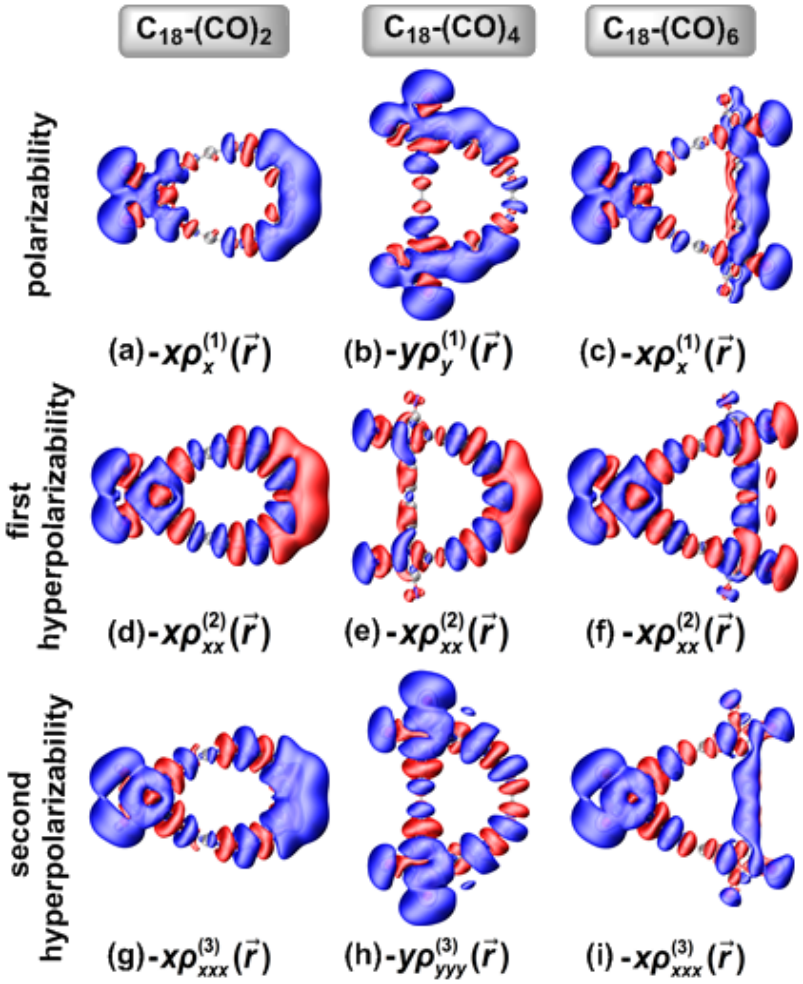

Fig. 6. Local contribution map of (hyper)polarizabilities of C_{18}-$(CO)_n$ (n = 2, 4, and 6) in direction with their largest tensorial component in static electric field. Blue and red isosurfaces represent positive and negative contribution regions, respectively. The isovalues of polarizability, first hyperpolarizability, and second hyperpolarizability are set to be 0.2, 2.5, and 200.0 au, respectively.

The local contributions of the (hyper)polarizability of the C_{18}-$(CO)_n$ (n = 2, 4, and 6)

in two axes except the direction with their largest tensorial component in static electric field were also studied, see **Figs. S3** and **S4,** respectively, for comparison. It can be observed that the (hyper)polarizability density isosurfaces of these two tensorial components are obviously narrow, especially for the first and second hyperpolarizabilities. And even more, under the same isovalue, the isosurfaces of Z-tensorial component are not even visible at all. A good correspondence is found between the isosurface features and the response values on these two axes, as in the case of the major tensorial components of (hyper)polarizability discussed above.

We also integrated the (hyper)polarizability densities illustrated in **Fig. 6** in the space of every atom based on the Becke's partition to quantitatively study the contribution of fragments to the major (hyper)polarizability tensorial components [43,44]. Each molecule is divided into two substructures, C_{18} moiety and -$(CO)_n$ group, and the corresponding results are plotted in **Fig. 7**.

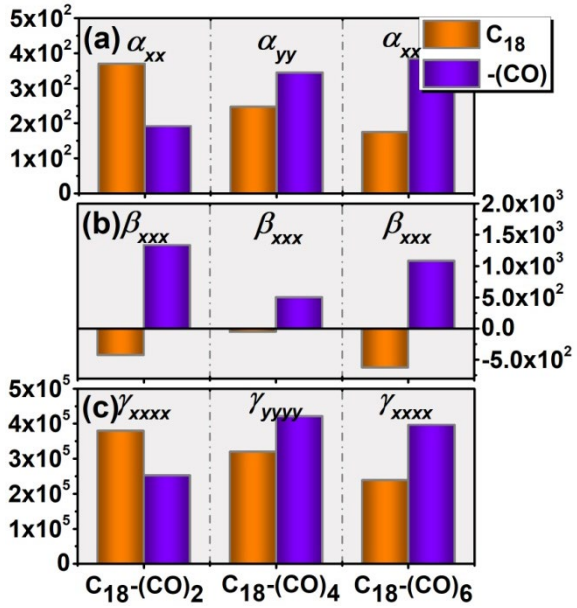

Fig. 7. Decomposition of the major tensorial components of (hyper)polarizabilities of C_{18}-$(CO)_n$ (n = 2, 4, and 6) into contributions from C_{18} moiety and -$(CO)_n$ group. The (hyper)polarizabilities are given in au.

According to **Fig. 7**, from the perspective of fragment contribution, the two fragments of the precursors C_{18}-$(CO)_n$ (n = 2, 4, and 6) all make significant contributions to the major tensorial components of (hyper)polarizability of the

molecule. Moreover, with the increasing number of the -CO groups in molecule, the contribution of the -$(CO)_n$ group to the molecular (hyper)polarizability increases, while the contribution of the C_{18} moiety gradually decreases. These results show once again that the introduction of -CO groups in the carbon ring can not only change the optical nonlinearity of the system, but also, more importantly, the (hyper)polarizability of the molecule can be regulated by controlling the number of -CO groups.

3.2.2 Dynamic (Hyper)Polarizability

Since the response properties of direct experimental observation are usually the frequency-dependent (hyper)polarizabilities measured in an external electric field at a certain frequency, we also calculated the dynamic (hyper)polarizabilities under the incident lights most commonly used in experiments. The values under the external fields of λ = 1907, 1460, 1340, 1180, and 1064 nm are given in **Tables S1** and **S2**, where the isotropic average polarizability [$\alpha_{iso}(\lambda)$], the projection of first hyperpolarizability on molecular dipole [$\beta_{vec}(\lambda)$], and the average of second hyperpolarizability [$\gamma_{||}(\lambda)$] correspond to $\alpha_{iso}(-\omega,\omega)$, $\beta_{vec}(-2\omega;\omega,\omega)$, and $\gamma_{||}(-2\omega;\omega,\omega,0)$, respectively. The $\alpha_{iso}(\lambda)$, $\beta_{vec}(\lambda)$, and $\gamma_{||}(\lambda)$ at various frequencies are collectively plotted in **Fig. 8**. It is found that for molecules C_{18}-$(CO)_n$ (n = 2, 4, and 6) with different numbers of -CO groups, their dynamic (hyper)polarizabilities show a completely consistent trend with the static cases. It can also be seen that the hyperpolarizabilities of C_{18}-$(CO)_n$ (n = 2, 4, and 6) show strong polarization resonance effect in the dynamic fields, as the hyperpolarizabilities increase markedly with the frequency of the external field. While by comparison, the polarizabilities of these molecules are quite insensitive to the external field frequency. It is noted that the dispersion of the optical nonlinearity reaches the maximum at 1064 nm in the current study.

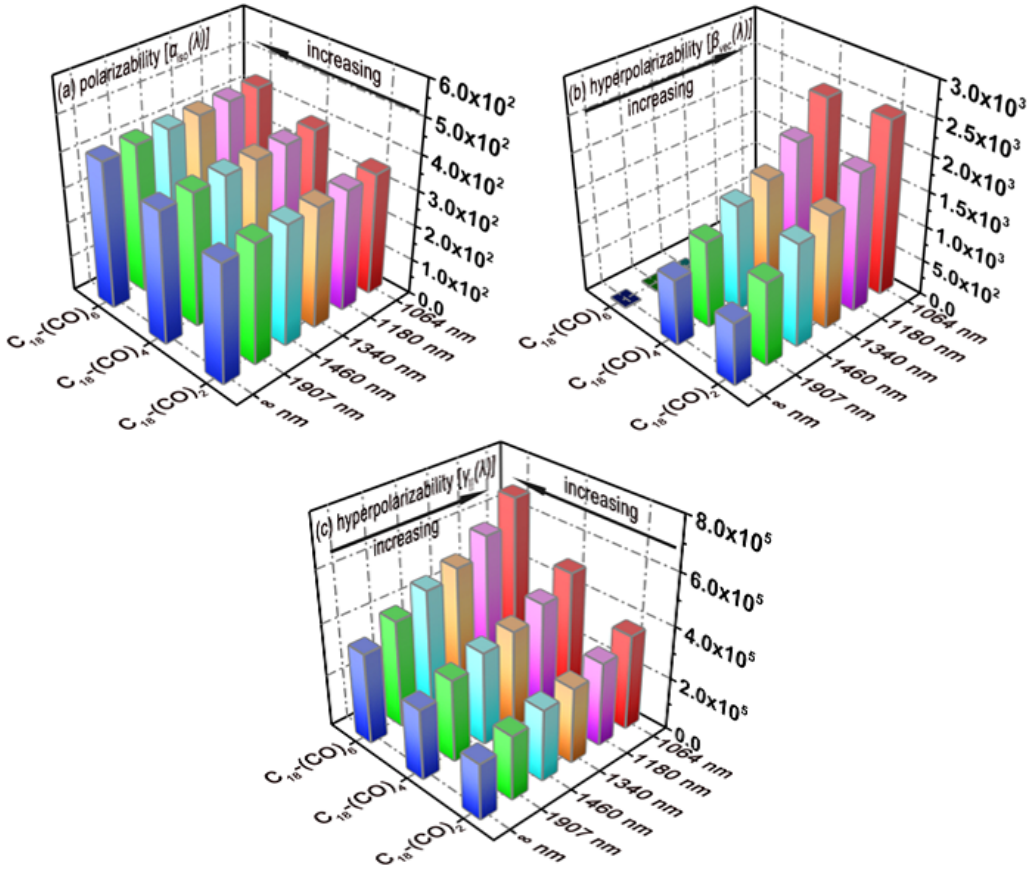

Fig. 8. (a) Isotropic average polarizability [$\alpha_{iso}(\lambda)$], (b) projection of first hyperpolarizability on molecule dipole [$\beta_{vec}(\lambda)$], and (c) average of second hyperpolarizability [$\gamma_{\|}(\lambda)$] of C_{18}-$(CO)_n$ (n = 2, 4, and 6) in zero-frequency limit ($\lambda = \infty$ nm) and under frequency-dependent fields (λ = 1907, 1460, 1340, 1180, and 1064 nm). The (hyper)polarizabilities are given in au.

4. Conclusions

The photophysical property and optical nonlinearity of C_{18} precursors, C_{18}-$(CO)_n$ (n = 2, 4, and 6), were assessed comprehensively by combining quantum chemistry calculations and wavefunction analyses. The results revealed that the red-shift of the absorption spectrum occurs with the increase of the number of -CO groups in the molecules, and the intrinsic contribution to the overall absorption spectrum is as follows: electronic local excitation within the C_{18} ring > electron transfer from the -$(CO)_n$ group to the C_{18} ring > electron transfer from the C_{18} ring to the -$(CO)_n$ group > electronic local excitation within the -$(CO)_n$ group. Due the planar configuration of

the studied precursors, their (hyper)polarizabilities show significant anisotropy, reflecting in the observation that the tensorial components in a specific axis of the molecule are more dominant than those along the other directions. The first and second hyperpolarizabilities of the molecules show obvious polarization resonance effect under the frequency-dependent external electric fields, but insignificant effect of molecular polarizability by external field frequencies was observed. Changing the number of -CO groups in molecules not only affects the (hyper)polarizability of C_{18}-$(CO)_n$ (n = 2, 4, and 6), but also changes the contribution source of molecular nonlinear responses, which demonstrates that the optical nonlinearity of the molecules can be regulated by introducing different number of -CO groups. The reason for the discrepancy of (hyper)polarizability of different molecules studied are clarified from the perspectives of the physical and structural origins by means of (hyper)polarizability density analysis and (hyper)polarizability contribution decomposition, respectively.

This work provides some physical perspectives for understanding the essence of optical properties of C_{18}-$(CO)_n$ (n = 2, 4, and 6), which will be conducive to rationally design advanced functional molecules with high performance based on sp-hybridized carbon-rich rings and further exploring their potential applications in optical materials.

Acknowledgments

This work was supported by National Natural Science Foundation of China for Youths (21701059) and Natural Science Foundation of Jiangsu Province for Youths (BK20170571).

References

[1] R. Hoffmann, Extended Hückel theory-v Cumulenes, polyenes, polyacetylenes and Cn, Tetrahedron 22 (2) (1966) 521–538.

[2] F. Diederich, Y. Rubin, C.B. Knobler, R.L. Whetten, K.E. Schriver, K.N. Houk, et

al, All-carbon molecules: Evidence for the generation of cyclo[18]carbon from a stable organic precursor, Science 245 (4922) (1989) 1088–1090.

[3] Y. Rubin, C. B. Knobler, F. Diederich, Synthesis and crystal structure of a stable hexacobalt complex of cyclo[18]carbon, J. Am. Chem. Soc. 112 (1990) 4966–4968.

[4] S. W. McElvany, M. M. Ross, N. S. Goroff, F. Diederich, Cyclocarbon coalescence: Mechanisms for tailor-made fullerene formation, Science 259 (1993) 1594–1596.

[5] G. von Helden, N. G. Gotts, M. T. Bowers, Experimental evidence for the formation of fullerenes by collisional heating of carbon rings in the gas phase, Nature 363 (1993) 60–63.

[6] F. Diederich, M. Kivala, All-carbon scaffolds by rational design, Adv. Mater. 22 (2010) 803–812.

[7] N. Pavliček, P. Gawel, D. R. Kohn, Z. Majzik, Y. Xiong, G. Meyer, H. L. Anderson, L. Gross, Polyyne formation via skeletal rearrangement induced by atomic manipulation, Nat. Chem. 010 (2018) 853–858.

[8] K. Kaiser, L.M. Scriven, F. Schulz, P. Gawel, L. Gross, H.L. Anderson, An sp-hybridized molecular carbon allotrope, cyclo[18]carbon, Science 365 (6459) (2019) 1299–1301.

[9] Z. Liu, T. Lu, Q. Chen, An sp-hybridized all-carboatomic ring, cyclo[18]carbon: Bonding character, electron delocalization, and aromaticity, Carbon 165 (2020) 468–475.

[10] Z. Liu, T. Lu, A. Yuan, X. Wang, Q. Chen, X. Yan, Remarkable size effect on photophysical and nonlinear optical properties of all-carboatomic rings, cyclo[18]carbon and its analogues, Chem. Asian. J. 16 (2021) 2267–2271.

[11] Z. Liu, T. Lu, Q. Chen, An sp-hybridized all-carboatomic ring, cyclo[18]carbon: Electronic structure, electronic spectrum, and optical nonlinearity, Carbon 165 (2020) 461–467.

[12] G.V. Baryshnikov, R.R. Valiev, A.V. Kuklin, D. Sundholm, H, Ågren, Cyclo[18]carbon: Insight into electronic structure, aromaticity and surface coupling, J.

Phys. Chem. Lett. 10 (2019) 6701–6705.

[13] Z. Liu, T. Lu, Q. Chen, Vibrational spectra and molecular vibrational behaviors of all-carboatomic rings, cyclo[18]carbon and its analogues, Chem. Asian. J. 16 (2021) 56–63.

[14] Z. Liu, T. Lu, Q. Chen, Intermolecular interaction characteristics of the all-carboatomic ring, cyclo[18]carbon: Focusing on molecular adsorption and stacking, Carbon 171 (2021) 514–523.

[15] T. Lu, Q. Chen, Ultrastrong regulation effect of electric field on all-carboatomic ring, cyclo[18]carbon, ChemPhysChem 22 (2021) 386–395.

[16] Z. Liu, T. Lu, Q. Chen, Comment on "Theoretical investigation on bond and spectrum of cyclo[18]carbon (C_{18}) with sp-hybridized", J. Mol. Model. 27 (2021) 42.

[17] S. Fang, Y. Hu, Cyclo[18]carbon as an ultra-elastic molecular O-ring with unique mechanical properties, Carbon 171 (2021) 96–103.

[18] C. Dai, D. Chen, J. Zhu, Achieving adaptive aromaticity in cyclo[10]carbon by screening cyclo[*n*]carbon (*n* = 8–24), Chem. Asian. J. 15 (14) (2020) 2187–2191.

[19] T. Lu, Z. Liu, Q. Chen, Comment on "18 and 12 – Member carbon rings (cyclo[*n*]carbons) – A density functional study", Mat. Sci. Eng. B 273 (2021) 115425.

[20] S. Kozuch, A. Nandi, E. Solel, Carbon tunneling in the automerization of cyclo[18]carbon, Chem. Eur. J. 26 (3) (2020) 564–753.

[21] A.E. Raeber, D.A. Mazziotti, Non-equilibrium steady state conductivity in cyclo[18]carbon and its boron nitride analogue, Phys. Chem. Chem. Phys. 22 (41) (2020) 23998–24003.

[22] Y. Jiang, E.J. Mattioli, M. Calvaresi, Z. Wang, Theoretical design of an ultrafast supramolecular rotor composed of carbon nano-rings, Chem. Commun. 56 (79) (2020) 11835–11838.

[23] A.J. Stasyuk, O.A. Stasyuk, M. Solà, A.A. Voityuk, Cyclo[18]carbon: The smallest all-carbon electron acceptor, Chem. Commun. 56 (3) (2020) 352−355.

[24] L.M. Scriven, K. Kaiser, F. Schulz, A.J. Sterling, S.L. Woltering, P. Gawel, K.E. Christensen, H.L. Anderson, L. Gross, Synthesis of cyclo[18]carbon via

debromination of $C_{18}Br_6$, J. Am. Chem. Soc. 142 (30) (2020) 12921–12924.

[25] Y. Rubin, C.B. Knobler, F. Diederich, Precursors to the cyclo[*n*]carbons: From 3.4-dialkynyl-3-cyclobutene-1,2-diones and 3.4-dialkynyl-3-cyclobutene-1,2-diols to cyclobutenodehydroannulenes and fligher oxides of carbon, J. Am. Chem. Soc. 112 (4) (1990) 1607–1617.

[26] Y. Rubin, M. Kahr, C.B. Knobler, F. Diederich, C.L.Wilkins, The higher oxides of carbon $C_{8n}O_{2n}$ (n = 3–5): Synthesis, characterization, and X-ray crystal structure. Formation of cyclo[*n*]carbon ions C_n^+ (n = 18, 24), C_n^- (n = 18, 24, 30), and higher carbon ions including C_{60}^+ in laser desorption Fourier transform mass spectrometric experiments, J, Am. Chem. Soc. 113 (2) (1991) 495–500.

[27] Z. Liu, S. Hua, X. Yan, Linear and nonlinear optical properties of triphenylamine−indandione chromophores: Theoretical study of the structure−function relationship under the combined action of substituent and symmetry change, J. Phys. Chem. A 122 (2018) 2344−2352.

[28] X. Wang, Z. Liu, X. Yan, T. Lu, W. Xiong, Bonding character, electron delocalization, and aromaticity of cyclo[18]carbon (C_{18}) precursors C_{18}-$(CO)_n$ (n = 6, 4, and 2): Focusing on the effect of -CO groups, ChemRxiv (2021) DOI: 10.33774/chemrxiv-2021-01pw7-v2.

[29] J.-D. Chai, M. Head-Gordon, Long-range corrected hybrid density functionals with damped atom-atom dispersion corrections, Phys. Chem. Chem. Phys. 10 (44) (2008) 6615–6620.

[30] F. Weigend, R. Ahlrichs, Balanced Basis Set of Split Valence, Triple zeta and quadruple zeta valence quality for H to Rn: Design and assessment of accuracy, Phys. Chem. Chem. Phys. 7 (2005) 3297–3305.

[31] T.H. Dunning Jr., Gaussian basis sets for use in correlated molecular calculations. I. The atoms boron through neon and hydrogen, J. Chem. Phys. 90 (1989) 1007–1023.

[32] M.J. Frisch, G.W. Trucks, H.B. Schlegel, G.E. Scuseria, M.A. Robb, J.R. Cheeseman, et al., Gaussian 16, revision A.03; Gaussian, Inc.: Wallingford, CT, 2016.

[33] T. Lu, F. Chen, Multiwfn: A multifunctional wavefunction analyzer, J. Comput.

Chem. 33 (2012) 580–592.

[34] T. Lu, Multiwfn manual, version 3.8(dev), Section 3.21.8, available at http://sobereva.com/multiwfn (accessed on Mar 30, 2021)

[35] W. Humphrey, A. Dalke, K. Schulten, VMD: Visual molecular dynamics, J. Mol. Graphics 14 (1996) 33–38.

[36] Z. Liu, Z. Tian, T. Lu, S. Hua, Theoretical framework of 1,3-thiazolium-5-thiolates mesoionic compounds: Exploring the nature of photophysical property and molecular nonlinearity, J. Phys. Chem. A 124 (2020) 5563–5569.

[37] Z. Liu, T. Lu, Optical properties of novel conjugated nanohoops: Revealing the effects of topology and size, J. Phys. Chem. C 124 (2020) 7353–7360.

[38] Z. Liu, T. Lu, Controllable photophysical and nonlinear properties in conformation isomerization of macrocyclic [32]octaphyrin(1.0.1.0.1.0.1.0) involving Hückel and Möbius topologies, J. Phys. Chem. C 124 (2020) 845–853.

[39] Z. Liu, X. Wang, T. Lu, A. Yuan, X. Yan, Tuning electronic structure and optical properties of Li@cyclo[18]carbon complex via switching doping position of lithium atom, ChemRxiv (2021) DOI: 10.26434/chemrxiv.14601168.

[40] T. Brinck, J. S. Murray, P. Politzer, Polarizability and volume, J. Chem. Phys. 98 (1993) 4305–4306.

[41] A. Tuer, S. Krouglov, R. Cisek, D. Tokarz, V. Barzda, Three-dimensional visualization of the first hyperpolarizability tensor, J. Comput. Chem. 32 (2011) 1128−1134.

[42] Z. Liu, S. Hua, G. Wu, Extended first hyperpolarizability of quasi-octupolar molecules by halogenated methylation: Whether the iodine atom is the best choice, J. Phys. Chem. C 2018 122 (37) (2018) 21548−21556.

[43] A.D. Becke, A multicenter numerical integration scheme for polyatomic molecules, J. Chem. Phys. 88 (1988) 2547–2553.

[44] T. Lu, F. Chen, Bond Order Analysis Based on the Laplacian of Electron Density in Fuzzy Overlap Space, J. Phys. Chem. A 117 (14) (2013) 3100–3108.